Local Non-Esterified Fatty Acids Correlate With Inflammation in Atheroma Plaques of Patients With Type 2 Diabetes

Sebastián Mas,[1] Roxana Martínez-Pinna,[1] Jose Luis Martín-Ventura,[1] Raul Pérez,[2] Dulcenombre Gomez-Garre,[3] Alberto Ortiz,[1] Arturo Fernandez-Cruz,[3] Fernando Vivanco,[4] and Jesús Egido[1]

OBJECTIVE—Atherosclerosis is prevalent in diabetic patients, but there is little information on the localization of nonesterified fatty acids (NEFAs) within the plaque and their relationship with inflammation. We sought to characterize the NEFA composition and location in human diabetic atheroma plaques by metabolomic analysis and imaging and to address their relationship with inflammation activity.

RESEARCH DESIGN AND METHODS—Time-of-flight secondary ion mass spectrometry (TOF-SIMS) was used for metabolomic analysis imaging of frozen carotid atheroma plaques. Carotid endarterectomy specimens were used for conventional immunohistochemistry, laser-capture microdissection quantitative PCR, and in situ Southwestern hybridization. Biological actions of linoleic acid were studied in cultured vascular smooth muscle cells (VSMCs).

RESULTS—TOF-SIMS imaging evidenced a significant increase in the quantity of several NEFA in diabetic versus nondiabetic atheroma plaques. Higher levels of NEFA were also found in diabetic sera. The presence of LPL mRNA in NEFA-rich areas of the atheroma plaque, as well as the lack of correlation between serum and plaque NEFA, suggests a local origin for plaque NEFA. The pattern of distribution of plaque NEFA is similar to that of MCP-1, LPL, and activated NF-κB. Diabetic endarterectomy specimens showed higher numbers of infiltrating macrophages and T-lymphocytes—a finding that associated with higher NEFA levels. Finally, linoleic acid activates NF-κB and upregulates NF-κB–mediated LPL and MCP-1 expression in cultured VSMC.

DISCUSSION—There is an increased presence of NEFA in diabetic plaque neointima. NEFA levels are higher in diabetic atheroma plaques than in nondiabetic subjects. We hypothesize that NEFA may be produced locally and contribute to local inflammation. *Diabetes* **59:1292–1301, 2010**

The costs of publication of this article were defrayed in part by the payment of page charges. This article must therefore be hereby marked "advertisement" in accordance with 18 U.S.C. Section 1734 solely to indicate this fact.

Atherosclerosis is the major cause of death among diabetic patients, accounting for 50% of mortality (1). Diabetes-associated atherosclerosis has been estimated to affect 5–8% of the general population and is by itself a major cause of death and disability in developed countries. Many factors have been postulated to link both conditions. Among these factors we find the proinflammatory and cytotoxic actions of high glucose levels and the generation of advanced glycation end products of proteins that may result in protein dysfunction or activation of the receptor for advanced glycation end products (2,3). Lipid abnormalities also contribute to diabetes-associated atherosclerosis and even to insulin resistance (4). Dyslipidemia is associated with increased lipolysis and the release of higher amounts of nonesterified fatty acids (NEFAs) into the bloodstream (5). Hyperglycemia creates a feedback loop, increasing lipolysis (6,7) and leading to a chronic exposure to NEFA. Plasma NEFAs promote a systemic insulin resistance state susceptible to being modified by dietary or therapeutic intervention using fat-poor diets or hypolipidemic agents (8). Central obesity has been linked to predisposition to type 2 diabetes, possibly through an increased lipolysis at visceral adipose tissue compared with subcutaneous adipocytes (9).

Despite the vast amount of evidence on the role that elevated serum levels of NEFA play on the development of vascular damage in diabetes (10), very little is known about their accumulation on the arterial wall. NEFAs have been linked to changes in matrix proteoglycans leading to an increased lipoprotein uptake on the arterial wall (11). Emerging molecular imaging techniques, such as TOF-SIMS, rely on direct interfacing between thin tissue slices and a mass spectrometer as a detector, allowing precise measurements of previously unknown molecules (12,13). Cluster TOF-SIMS has a strong bias toward hydrophobic molecules, displaying high-resolution images of the most abundant lipids present on the sample surface. Additionally, minimal manipulation of snap-frozen samples prevents analyte delocalization, critical for accurate colocalizations, allowing a straightforward integration with other histological techniques.

We used TOF-SIMS to characterize the presence and distribution of NEFA in atheroma plaque specimens from diabetic and nondiabetic subjects. The diabetic plaque samples had a more severe degree of inflammation and a higher amount of certain NEFA, including linoleic acid. NEFA colocalized with lipoprotein lipase (LPL) and mono-

TABLE 1
Baseline clinical characteristics of study participants

	Diabetic	Nondiabetic	P
Age (years)	71 ± 8	72 ± 9	NS
Sex (male/female)	16/3	18/3	NS
Hypertension	13/19	11/21	NS
Hypercholesterolemia	14/19	12/21	NS
Smoking	9/19	10/21	NS

Data are means $\pm$ SD unless otherwise indicated.

cyte chemoattractant protein (MCP)-1 expression in plaques and, in cultured vascular smooth muscle cells (VSMCs), linoleic acid promoted nuclear factor-κB (NF-κB) activation and LPL and MCP-1 expression.

RESEARCH DESIGN AND METHODS

A total of 40 consecutive patients undergoing carotid endarterectomy (>70% carotid stenosis) at the Vascular Surgery Units of Hospital Clínico San Carlos and Fundación Jimenez Díaz were studied. The study was approved by the local ethics committees in accordance with international guidelines, and informed consent was obtained before enrollment.

Basic patient characteristics are shown in Table 1. There were no differences between patients with type 2 diabetes and nondiabetic subjects in age, sex, or prevalence of hypertension, hypercholesterolemia, or smoking. Atherosclerotic plaques obtained during surgery were immediately processed for further studies. The first four diabetic and first four nondiabetic subject samples were snap-frozen immediately and named the "test group" and the next 32 collected were embedded in paraffin and named the "validation group." Both groups had similar clinical characteristics. Clinical data from the TOF-SIMS group are shown in Table 2. Blood samples for biochemical analysis were drawn before the surgical procedure. NEFAs were determined using the NEFA C enzymatic assay kit (WAKO, Neuss, Germany).

TOF-SIMS. Samples were kept at −80°C until 10-μm slices were cut using a cryostat (CM1900; Leica) at a constant temperature of −25°C. Tissue sections were deposited onto a stainless steel plate (15-7PH; Goodfellow) and stored again at −80°C. After drying under a pressure of a few hPa for 15 min, they were directly analyzed in a TOF-SIMS V mass spectrometer (IonTof, Germany) fitted with a bismuth cluster ion source located at the Parque Científico de Barcelona.

The primary ions impinge the surface of the tissue section with a kinetic energy of 25 keV. The primary ion dose was between 4.7×10^{11} and 10^{12} ions/cm2. The secondary ions were extracted with 2 keV energy and postaccelerated to 10 keV just before hitting the detector surface (single-channel plate followed by a scintillator and a photomultiplier). A low-energy electron flood gun was activated to neutralize the surface during the analysis. The effective ion flight path is ~2 m using a reflectron, and the mass resolution is ~6,300 (full width at half-maximum) at a mass-to-charge ratio (m/z) of 35 and 10,000 at 795.7 m/z.

The field of view is $8,000 \times 8,000 \ \mu m^2$ (512×512 pixels). The name of the compounds or the m/z value of the peak centroid, the maximal number of counts in a pixel, and the total number of counts are written below each image. The color scales correspond to the interval [0, maximal number of counts in a pixel].

Mass calibration and ion peak identifications were performed as has previously been described (13). Briefly, initial calibration of monatomic hydrogen was performed, followed by sequential calibration of known molecules up to 882 Da. In this study, we focus only on previously identified quasimolecular ions (14). Total arterial wall NEFA was calculated as the mean of the different NEFA values normalized by the surface of the sample.

Laser capture microdissection. Frozen endartery tissue was sectioned at 10 μm and mounted on a slide covered with a polyethylene naphthalate membrane (PALMZeiss Microlaser Technologies). Tissue slices were stained with hematoxylin-eosin. RNase-free conditions were maintained as completely as possible.

TOF-SIMS–directed areas of interest were collected by laser microdissection and pressure catapulting, which was performed using a PALM MicroLaser system (PALM-Zeiss) containing a PALM MicroBeam (driven by PALM Micro-Beam software) and a PALM RoboStage. A typical setting used for laser cutting was a beam size of 30 μm and laser strength of 30 mV under a $5\times$ ocular lens.

Dissected artery sections were catapulted directly into 25 μl RNAqueous microlysis solution, and total RNA was isolated according to the manufacturer's recommendations (RNAqueous micro RNA isolation kit, Ambion) and stored at −80°C until use. Samples from four patients were studied in each group (diabetic vs. nondiabetic) with at least three areas of interest per patient, with a total surface of 120,000 μm^2.

VSMC cultures. Human aortic VSMCs (CRL-1999; ATCC) were cultured in Ham's F-12 supplemented with 10% FBS, 2 mmol/l glutamine, 100 units/ml penicillin, 100 μg/ml streptomycin, ITS (2.5 μg/ml insulin from bovine pancreas, 2.5 μg/l human transferrine, and 2.5 ng/ml sodium selenite), and 30 μg/ml endothelial growth supplement at 37°C in 5% CO_2 as previously described (15). Cells between passages three and seven were used for all experiments. Certain experiments were replicated in primary cultures of rat VSMC.

RNA extraction and real-time quantitative PCR. Total RNA from VSMC cultures was isolated using TRIzol Reagent (Invitrogen). One microgram of RNA was reverse transcribed with a High Capacity cDNA Archive kit (Applied Biosystems, Foster City, CA). RNA from tissue was isolated as described above. All real-time PCR reactions were performed on an ABI Prism 7500 sequence detection PCR system (Applied Biosystems) according to the manufacturer's protocol using the DeltaDelta Ct method (16). Expression levels are given as ratios to 18S. Predeveloped primer and probe assays were obtained for human 18S and MCP-1 and LPL from Applied Biosystems.

Immunohistochemistry. Carotid atherosclerotic plaques were stored in paraformaldehyde for 24 h and later in ethanol until paraffin embedding. Immunohistochemistry was performed as previously described (17). Primary antibodies were mouse anti-LPL antibody (Abcam), rabbit anti–MCP-1 anti-

TABLE 2
Baseline clinical characteristics of SIMS study participants

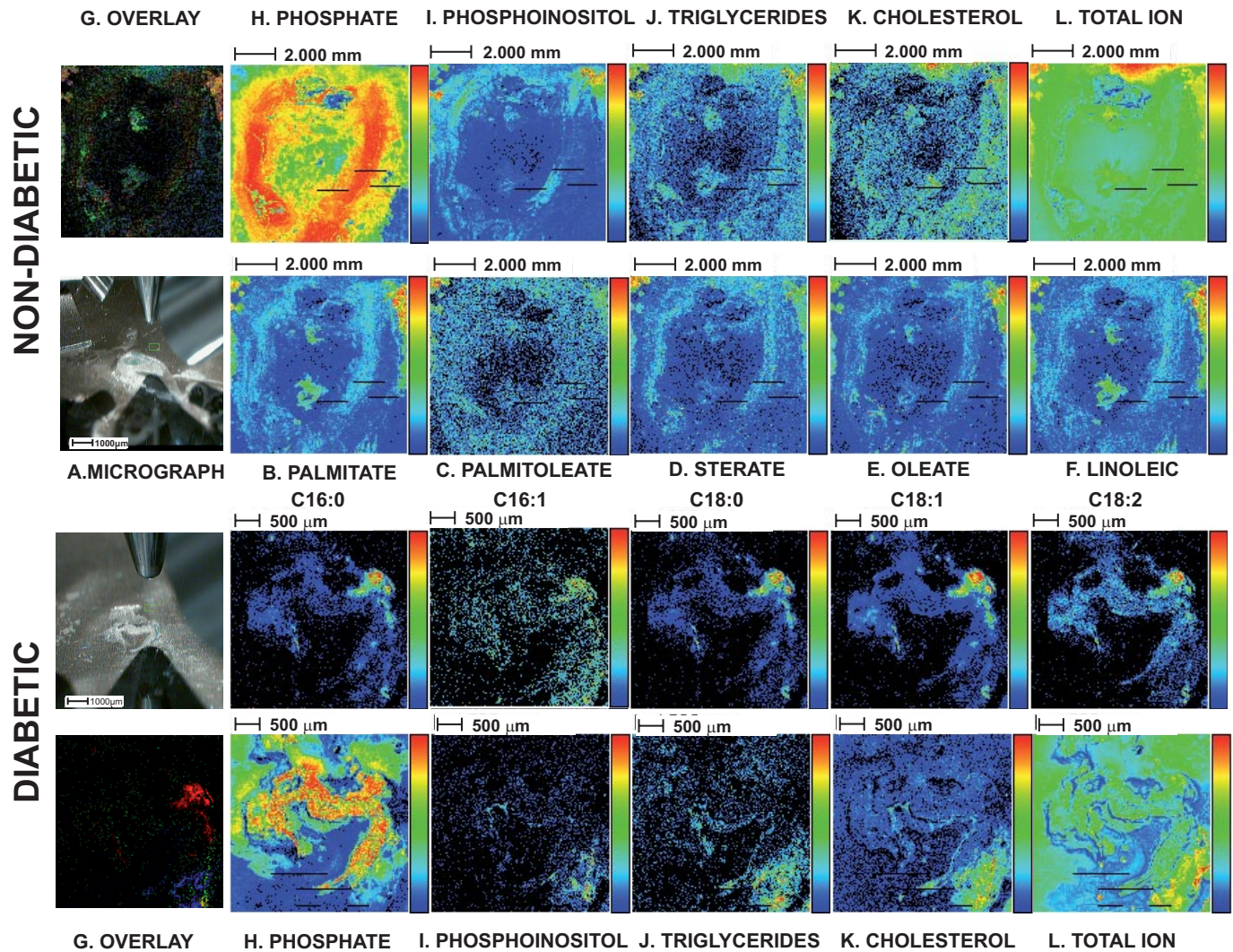|	Diabetic	Nondiabetic	P
Age (years)	71 ± 6.6	68.7 ± 8.7	NS
Sex (male/female)	4/0	3/1	NS
Smokers/total	3/4	2/4	NS
Glycemia (mg/dl)	170.5 ± 36.9	77.75 ± 8.2	<0.05
Insulin (μIU/dl)	26 ± 8	8.75 ± 1.6	<0.05
Systolic blood pressure (mmHg)	127.5 ± 14.7	122.5 ± 14.8	NS
Diastolic blood pressure (mmHg)	63.7 ± 9.6	65 ± 3.5	NS
HDL cholesterol (mg/dl)	66.5 ± 28	82 ± 3	NS
LDL cholesterol (mg/dl)	46.5 ± 16.5	41 ± 4.6	NS
Plasma cholesterol (mg/dl)	132 ± 42	140 ± 5	NS
Plasma triglycerides (mg/dl)	99.8 ± 40	89 ± 24.6	NS
Apolipoprotein A (mg/dl)	104.5 ± 32	106 ± 21	NS
Apolipoprotein B (mg/dl)	58.5 ± 15	65.6 ± 9.2	NS
Plasma NEFA (mg/dl)	24 ± 20.16	14 ± 5.73	NS
Tissue NEFA (area NEFA/plaque size)	0.142 ± 0.012	0.109 ± 0.004	<0.05
Plaque size (μm^2)	$1,835,000 \pm 873,500$	$2,540,000 \pm 873,000$	NS

Data are means $\pm$ SD unless otherwise indicated.

FIG. 1. Representative secondary ion images obtained from carotid endarteries obtained from a nondiabetic suject (*top panel*) and a diabetic subject (*bottom panel*) under the irradiation of bismuth cluster ions. From left to right: tissue micrograph (*A*); palmitate (C16:0) (*B*); palmitoleate (C16:1) (*C*); stearate (C18:0) (*D*); oleate (C18:1) (*E*); linoleate (C18:2) (*F*); image overlay of palmiteleate (red), cholesterol (green), and triglycerides (blue) (*G*); phosphate (*H*), phosphoinositol fragment (*I*), triglycerides (*J*), cholesterol (*K*), and total ion intensity (*L*). The field of view is 8 × 8 mm at 15,625 μm/pixel. (A high-quality digital representation of this figure is available in the online issue.)

body (Immugenex), anti-smooth muscle cell α-actin (1A4; Dako), or anti-human macrophages (HAM-56; Dako). Negative controls using the corresponding IgG were included to check for nonspecific staining.

Computer-assisted morphometric analysis with the Olympus semiautomatic image-analysis system Micro Image software (version 1.0 for Windows) was performed by a pathologist who was blinded to the patient's group as previously described (18). Results are expressed as the percentage of positive staining per square millimeter.

NF-κB Southwestern. The distribution and DNA-binding activity of NF-κB in situ was detected using a digoxigenin-labeled double-stranded DNA probe with a specific NF-κB consensus sequence. Competition assays with 100-fold excess of unlabeled probe were used as negative controls. For colocalization studies, immunohistochemistry for macrophages was carried out on slides directly from the final wash of the Southwestern histochemistry protocol without allowing them to dry as previously described (19).

Electrophoretic mobility shift assay. Electrophoretic mobility shift assay (EMSA) for NF-κB DNA binding activity was performed with nuclear protein extracts from VSMC as previously described (20). The specificity of the assay was tested with a 100-fold excess of unlabeled NF-κB consensus oligonucleotide added to the ^{32}P-labeled probe-binding reaction.

Western blot and ELISA. Equal amounts (30 μg) of cell lysate protein were loaded onto 12.5% polyacrylamide gels, eletrophoresed, and transfered to nitocellulose membranes. Then, membranes were blocked with 7% milk powder in TBS-Tween for 1 h and incubated with anti-LPL (goat polyclonal sc-32382 used at 1:200; Santa Cruz Biotechnology), anti-IκBα (rabbit polyclonal sc-371 used at 1:1,000; Santa Cruz Biotechnology) antibodies overnight at 4°C. Membranes were washed with TBS-Tween and incubated with anti-goat, anti-mouse, or anti-rabbit antibodies (1:2000) for 1 h at room temperature. The signal was detected using a chemiluminiscence kit (GE Healthcare). ELISA for MCP-1 (BD Biosciences) detection in culture supernatant was performed according to the manufacturer's protocol.

Statistical analysis. Statistical analysis was performed with SPSS for Windows software package (version 17; SPSS, Chicago, IL). Results are expressed as means ± SD. In vitro experiments were performed at least three times. Statistical testing was performed with a two-tailed α level of 0.05. Differences between diabetic and nondiabetic endarterectomy samples were assessed by the Mann-Whitney nonparametric test. Spearman correlation coefficients were calculated for continuous characteristics.

RESULTS

Increased NEFA in diabetic atherosclerotic plaques. Atheroma plaque samples subjected to TOF-SIMS imaging analysis using bismuth clusters as the primary ion source render multiple secondary ions corresponding with some of the most abundant metabolites present on their surface (Fig. 1). Ionization using liquid ion guns is biased toward more hydrophobic metabolites rendering secondary ions. Therefore, we focused on surface analysis of lipids and lipid derivatives.
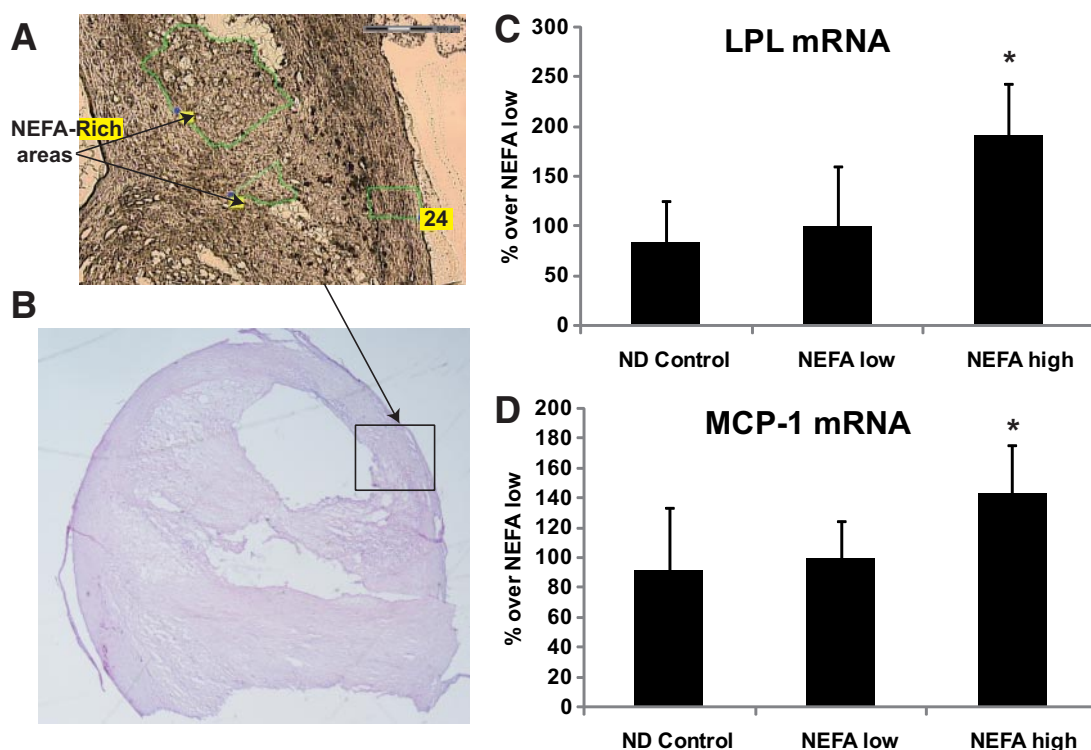
FIG. 2. LPL and proinflammatory cytokine mRNA expression in NEFA-rich areas. *A* and *B*: Hematoxilin-stained endarterectomy section for laser-capture microdissection showing NEFA-rich areas and its internal controls (24). LPL mRNA (*C*) and MCP-1 mRNA (*D*) levels (measured by quantitative reverse-transcription PCR) in NEFA-rich areas (*n* = 4), diabetic VSMC control areas (*n* = 6), and nondiabetic lipid-rich areas (*n* = 6) (microdissections; means ± 95% CI; $P < 0.05$).

As shown in Fig. 1*A*, a density plot of the inorganic phosphate (79 m/z) molecules can be created similarly to doing so for any conventional histological study. The presence of phosphate ion correlates with the presence of biological tissue and is comparable with the optical image in Fig. 2. Thus, the morphometric measurement of inorganic phosphate can be used to estimate the size of the specimens. All metabolite measurements are expressed as the ratio between the metabolite area and phosphate area in order to normalize size variation. The phosphate area average value was 1.835 vs. $2.54 \ \mathrm{e}^6 \pm 873,000 \ \mu\mathrm{m}^2$ in

diabetic versus nondiabetic subjects, respectively (P = not significant).

Quantization of the relative abundance of molecules can be calculated because their ionization efficiency is constant for the whole rastering. Significant differences between the molecules in diabetic and nondiabetic atheroma plaques were found in only 3 of the 16 molecules. These three molecules were linoleic acid, palmitic acid, and oleic acid.

The linoleate quasimolecular ion (m/z) was consistently increased in all diabetic samples analyzed (C18:2) (0.135 ±

TABLE 3

Most abundant quasimolecular ions identified in atherosclerotic plaque negative spectrum

Molecule	Negative spectrum (m/z)	Signal in diabetic subjects	Signal in nondiabetic subjects	P
Phosphoinositol fragment	223.0051	0.342 ± 0.069	0.277 ± 0.067	NS
Phosphoinositol fragment	241.0147			
C16:0 (palmitic acid)	255.2314	0.211 ± 0.036	0.144 ± 0.033	$P < 0.05$
C16:1 (palmitoleic ac)	253.2195	0.043 ± 0.005	0.033 ± 0.010	NS
C16:2 (hexadecadioneic acid)	251.2052	—	—	NQ
C18:0 (stearic acid)	283.2609	0.213 ± 0.015	0.181 ± 0.008	NS
C18:1 (oleic acid)	281.2486	0.184 ± 0.078	0.106 ± 0.017	$P < 0.05$
C18:2 (linoleic acid)	279.2313	0.135 ± 0.034	0.083 ± 0.013	$P < 0.05$
C20:4 (arachidonic/eicosatetraenoic)	303.2353	—	—	NQ
Cholesterol	385.3467	0.092 ± 0.028	0.061 ± 0.024	NS
Vitamin E	429.3705	0.019 ± 0.008	0.012 ± 0.005	NS
Coenzyme Q9	795.6320	—	—	NQ
Phosphatidic acid	675.5013			
Phosphatidic acid	701.5270	0.357 ± 0.020	0.319 ± 0.021	NS
Triglycerides	829.7789			
Triglycerides	857.8163	0.380 ± 0.081	0.236 ± 0.050	NS

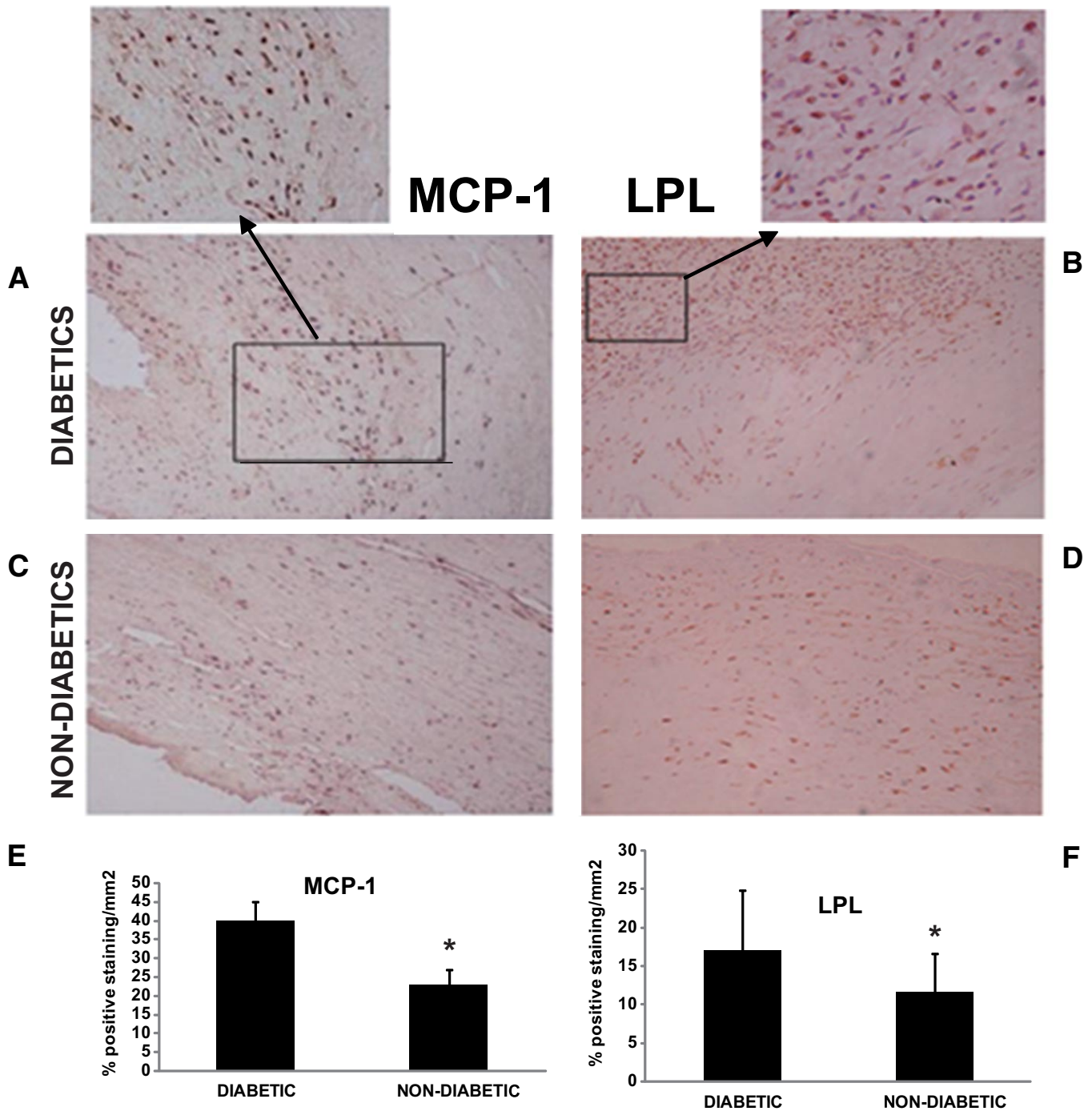Data are means ± SD unless otherwise indicated. NQ, nonquantitable.

FIG. 3. MCP-1 and LPL protein expression in diabetes. Representative examples of MCP-1 immunohistochemistry staining in a diabetic patient (*A*) and a nondiabetic atherosclerotic patient (*C*) and LPL immunohistochemistry in a diabetic patient (*B*) and a nondiabetic subject (*D*). Magnification of a highly positive area within the lesion is shown for both stainings. The protein expression shows a significant increase in the diabetic group vs. the nondiabetic for MCP-1 (*E*) and LPL (*F*). Vessels form healthy controls did not stain positive (data not shown). *$P < 0.05$.

0.034 vs. 0.083 ± 0.013 in diabetic and nondiabetic subjects, respectively; $P < 0.05$). Also, palmitic acid (C16:0) (0.211 ± 0.036 vs. 0.144 ± 0.033; $P < 0.05$) and oleic acid (C18:1) (0.184 ± 0.078 vs. 0.106 ± 0.017; $P < 0.05$) were significantly increased in plaques from the diabetic samples. As a control, synthetic triglycerides were irradiated at the ion dose used for analysis. Quantification of the in-source fragmentation rendered a negligible amount of NEFA (<10% of base peak). This effectively ruled out artifacts in NEFA measurement. The distribution pattern

was similar between the three fatty acids but did not fully overlap with triglyceride distribution.

Other lipids widely regarded as major players on atherosclerotic pathogenesis, such as cholesterol, did not significantly differ in quantity between diabetic and nondiabetic samples (Table 3). Furthermore, there were no differences in triglyceride accumulation (Table 3). Dyslipidemia in diabetes is mainly characterized by increased plasma triglyceride and NEFA levels (21,22). To test whether NEFA plasma levels correlate with arterial wall NEFA, we
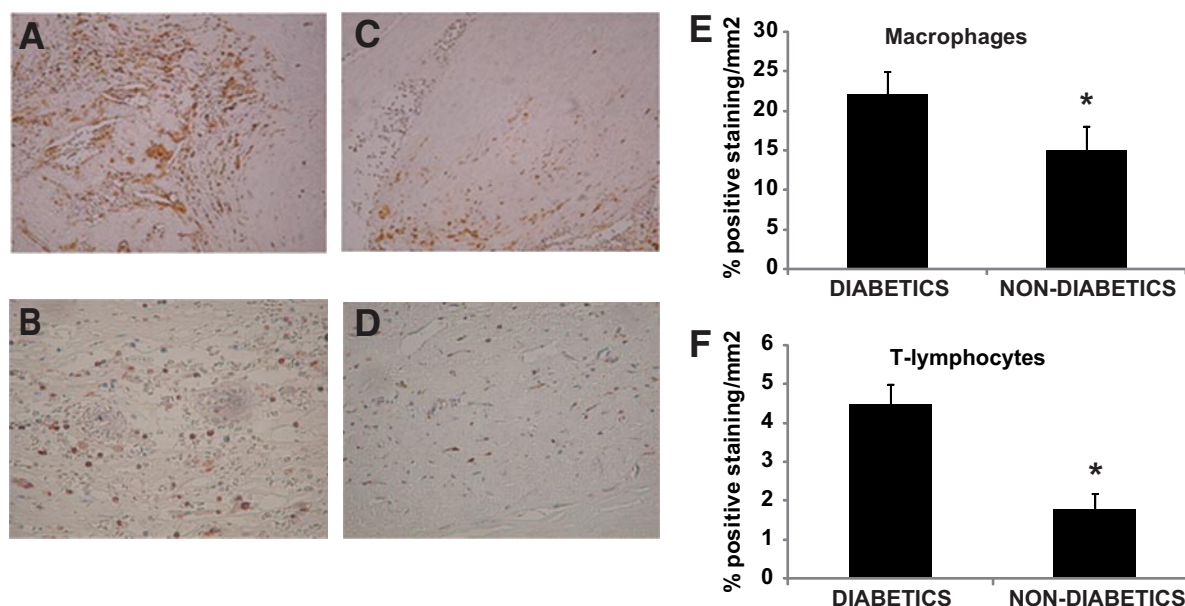
FIG. 4. Inflammatory cells in carotid atherosclerotic plaques studied by immunohistochemistry. Consecutive sections were stained for macrophages (*A* and *C*) and T-cells (*B* and *D*) on the plaque. Marked reductions in the number of positive cells within the intimae were observed in the nondiabetic group vs. the diabetic group both for macrophages (*C*) and T-cells (*D*). *E*: Macrophages. *F*: T-lymphocytes. *P < 0.05.

measured enzymatically both protein-bound and protein-free plasma fatty acids. Total fasting plasma NEFAs were higher in diabetic than in nondiabetic subjects (24.37 ± 20.16 vs. 14 ± 5.73 mg/dl, respectively; $P < 0.05$) (Table 1). We did not find any correlation between plasma NEFA and any of the lipid molecules measured by TOF-SIMS at the arterial wall (supplemental Table 1, available in an online appendix at http://diabetes.diabetesjournals.org/cgi/content/full/db09-0848/DC1). The sum of NEFA present on

the tissue correlated with glycemia but not with NEFA plasma levels (supplemental Table 1).

Lipoprotein lipase and MCP-1 expression on NEFA-rich areas. Several lipases promote the release of NEFA from complex lipids, mainly triglycerides. LPL is the major contributor to fatty acid hydrolysis in muscle and adipose tissue (23). High LPL expression by foam cells (24) plays a major role in local NEFA release in atherosclerotic vessels.

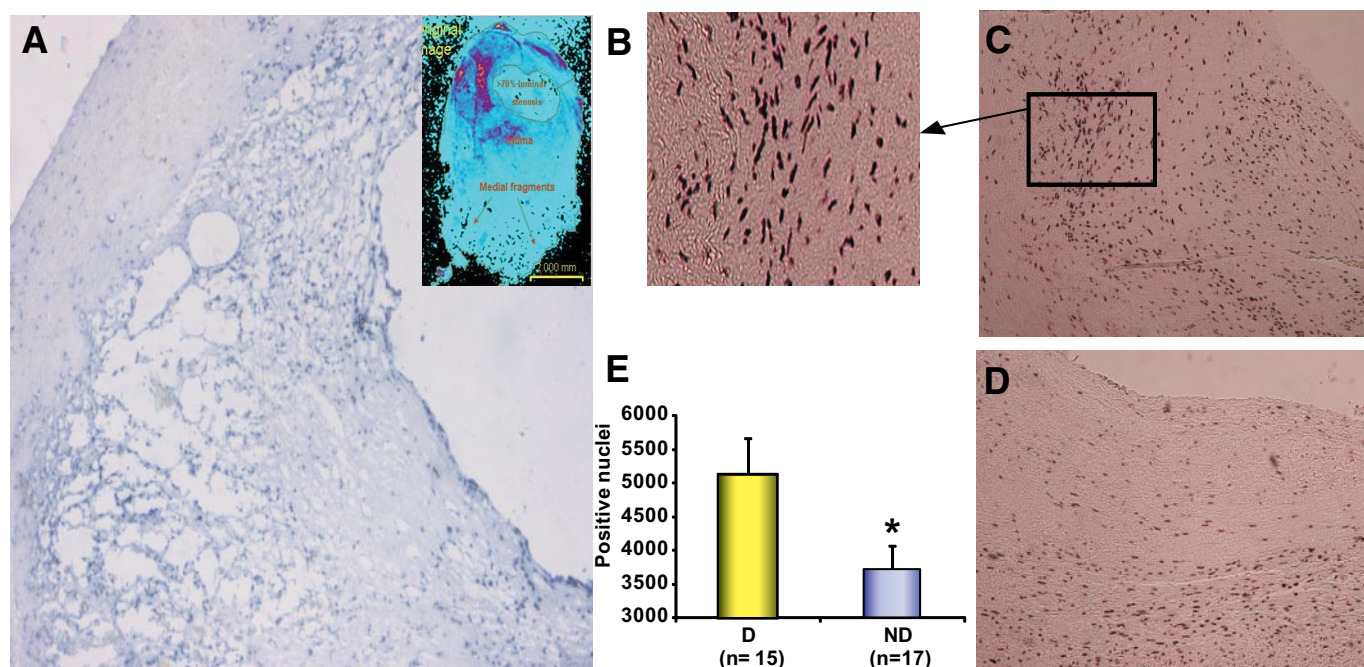We used laser-capture microdissection in slices consec-

FIG. 5. Arterial NF-κB activation determined by Southwestern histochemistry. Consecutive sections to those used in TOF-SIMS analysis (upper-right corner of *A*) were used for in situ southwestern (*A*). Purple nucleus indicates activation, showing a similar pattern of distribution. The measured intensity is similar to that observed in paraffin (*C* and *D*). The bar graph (*E*) shows the quantification of positive nuclei per millimeter squared in the lesions. *P* values refer to comparisons with nondiabetic subjects. Negative control showed no staining. *P < 0.05. (A high-quality digital representation of this figure is available in the online issue.)
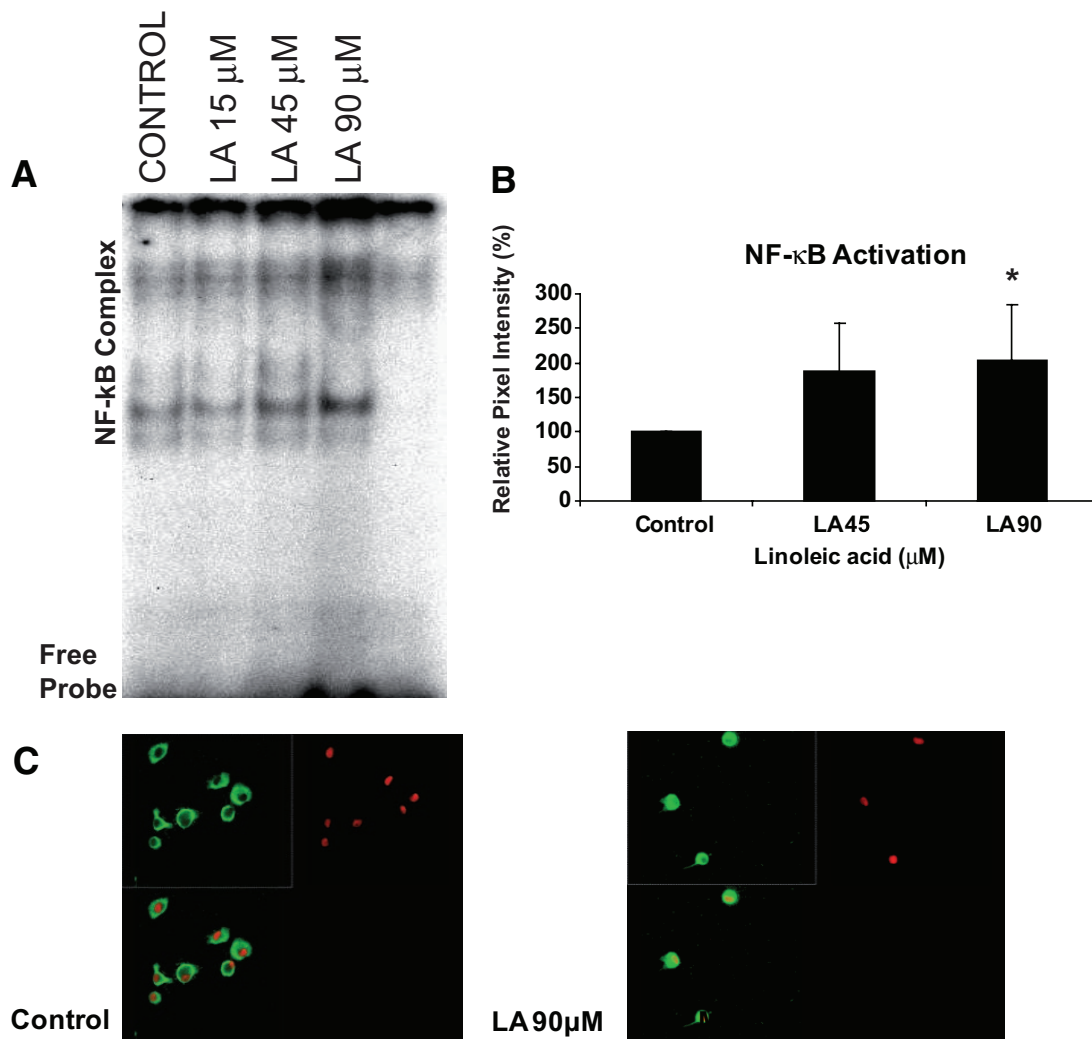
FIG. 6. NEFA induces NF-κB activation in VSMC. *A*: a representative EMSA is shown. *B*: Bar graph showing NF-κB activation in VSMCs incubated for 3 h with increasing linoleate (LA) concentrations. *C*: p65 subunit of NF-κB was detected by indirect immunostaining using FITC: Fluorescein isothiocyanate–labeled secondary antibodies and evaluated by confocal microscopy. Figure shows a representative experiment where rat VSMCs were incubated with or without 90 μmol/l linoleate. *$P < 0.05$. (A high-quality digital representation of this figure is available in the online issue.)

utive to those used for TOF-SIMS to quantify mRNA expression in NEFA-rich areas identified by TOF-SIMS imaging (Fig. 2*A*). A consistent increase (twofold; $P < 0.05$) in LPL mRNA expression was found in all diabetic NEFA-rich areas studied (Fig. 2*B*) in comparison with nondiabetic NEFA-rich areas and control diabetic NEFA-poor areas.

The expression of MCP-1 provides an insight into plaque-associated inflammation. MCP-1 mRNA and protein were quantitated by laser-capture microdissection qPCR (Fig. 2*D*) and by immunohistochemistry (Fig. 3*A*, *C*, and *E*), respectively. MCP-1 mRNA expression was higher in diabetic NEFA-rich areas (Fig. 2*D*). Diabetic subjects had a significantly higher percentage of MCP-1–immunostained neointimal area when compared with nondiabetic subjects (40 ± 5 vs. $23 \pm 4\%$, respectively; $P < 0.05$).

Immunohistochemical analysis of LPL expression was carried out in paraffin-embedded sections; the area immunostained for LPL was markedly higher in diabetic than in nondiabetic patients (17.1 ± 7.8 vs. $11.8 \pm 4.8\%$ of neointimal area; $P < 0.05$) (Fig. 3*B*, *D*, and *F*). Negative controls did not stain for LPL (not shown).

Macrophage and T-cell infiltration in atherosclerotic lesions. In relation to nondiabetic atherosclerotic samples, the diabetic group showed a significant increase of the percentage of neointima staining positive for macrophages (22 ± 3 vs. $15 \pm 3\%$; $P < 0.05$) (Fig. 4*A* and *C*) and T-cells (4.4 ± 2 vs. $1.8 \pm 0.5\%$; $P < 0.05$) (Fig. 4*B* and *D*), which is consistent with the increased chemokine expression. Those results are similar to those found in the literature (25).

NF-κB activation colocalizes with NEFA-rich areas. NF-κB activation was localized to NEFA-rich areas by Southwestern in frozen samples consecutive to those used for TOF-SIMS, allowing an overlay between them (Fig. 5*A* and *B*). In addition, a higher number of nuclei staining positive for NF-κB activation with Southwestern histochemistry was noted in paraffin-embedded diabetic atherosclerotic plaques than in nondiabetic subjects ($5,140 \pm 512$ vs. $3,738 \pm 316$ stained nuclei per mm^3; $P < 0.05$) (Fig. 5*C–E*). Nuclear staining was absent in negative controls (not shown).

Linoleic acid activates NF-κB in VSMC and upregulates LPL and MCP-1 expression. Additionally, we tested in cultured VSMC the possible functional relation
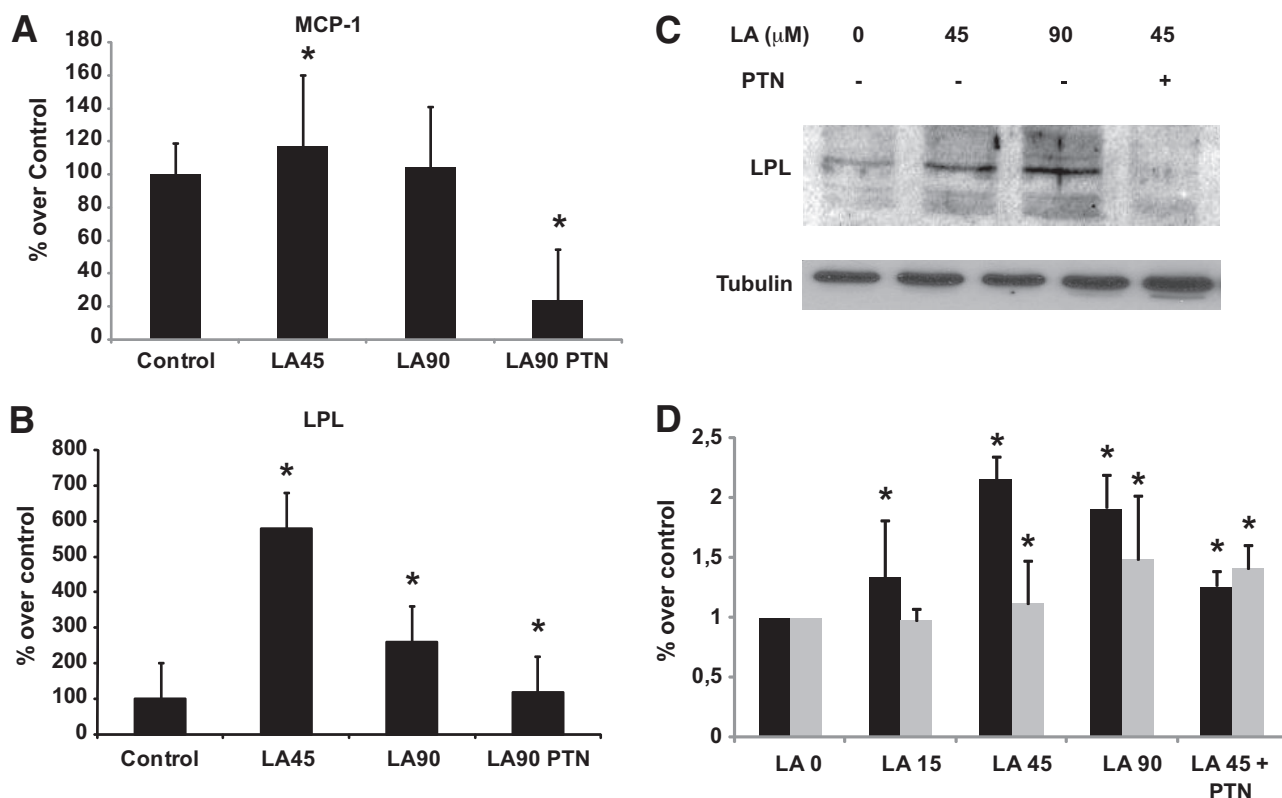
FIG. 7. Linoleic acid (LA) upregulates MCP-1 and LPL expression at the mRNA and protein level in cultured VSMC. MCP-1 (*A*) and LPL (*B*) transcript induction after exposure to different concentrations micromol (µmol/l) of linoleic acid for 3 h. *C*: Representative Western blot for LPL and tubulin as loading control. *D*: Quantitation of LPL (Western blot [black]) and MCP-1 (ELISA [gray]) protein expression. *$P < 0.05$. PTN, parthenolide.

between the observed colocalization of higher NEFA concentrations and NF-κB activation and LPL and MCP-1 upregulation. For these studies we chose linoleic acid, the NEFA with a highest increment in diabetic plaques (60% increase over that in nondiabetic subjects).

Linoleic acid increased the NF-κB DNA-binding activity in nuclear extracts, as assessed by EMSA (2.2-fold at 90 µmol/l linoleic acid; $P < 0.05$) (Fig. 6*A* and *B*). Confocal microscopy confirmed linoleic acid–induced NF-κB activation and nuclear translocation of p65 NF-κB (Fig. 6*C*).

Linoleic acid increased LPL and MCP-1 mRNA and protein, and this effect was prevented by pretreatment with 2.5 µg/ml parthenolide, an NF-κB inhibitor (28,29) (Fig. 7*A*–*D*) (28,29). This suggests that NF-κB mediates linoleic acid actions on VSMC.

DISCUSSION

Our group recently reported the use of TOF-SIMS to study the cartography of lipids in atherosclerotic plaques (13). We now report the presence of NEFA-rich areas within human atherosclerotic plaques. These NEFA-rich areas are especially prominent in diabetic subjects, and they colocalize with areas of inflammation characterized by NF-κB activation and increased LPL and MCP-1 expression.

The presence of NEFA-rich areas on the inner side of the endarterectomy specimens and its relation to inflammation is a novel finding, and very little is known about the mechanism involved. The extent of those NEFA-rich areas did not correlate with plasma NEFA levels, suggesting a local origin in the plaque. The distribution pattern of the three main fatty acids was similar but did not fully overlap

with triglyceride distribution or VLDL deposition (S. Mas, unpublished observation). This is consistent with the hypothesis that, in addition to triglycerides, other complex lipids could act as NEFA precursors. However, we cannot exclude the possibility of a triglyceride origin of NEFA. Several lipases such as LPL (30), endothelial lipase (31) and phospholipase A2 (32,33) activate and release NEFA on atherosclerotic lesions and contribute to vascular injury. LPL is considered the rate-limiting enzyme for hydrolysis of lipoprotein triglycerides (34), and it is likely to be secreted by macrophages within atherosclerotic lesions (24,35). The increased expression of LPL in the NEFA-rich areas suggests that NEFA might be generated locally by the action of this enzyme as lipid-laden macrophages become a major source of LPL (35). NEFA presence at the intima could be considered an indirect marker of macrophage infiltration. Nonetheless, image overlay shows a similar but not identical pattern for macrophages and NEFA, suggesting a contribution of other cell types, namely VSMC.

Diabetic patients had higher plaque levels of several NEFA probed (palmitic, linoleic, and oleic acids) despite cholesterol and triglyceride levels similar to those in nondiabetic subjects. In addition, diabetic subjects had evidence for higher plaque inflammation (25). Furthermore, NF-κB activation and increased expression of MCP-1 mRNA were noted in NEFA-rich areas. This raises the question of the relationship between NEFA and inflammation that may be bidirectional. LPL may be expressed in the context of inflammation (23). In addition, linoleic acid activated NF-κB and increased the expression of LPL and MCP-1 in cultured VSMC. Recently, linoleate induction of

cytokine expression by monocytes has been reported (36). The data are also consistent with the in vivo observation that an acute elevation of plasma NEFA activates the NF-κB pathway (37) and increases the hepatic expression of proinflammatory cytokines (38). NEFA may also contribute to vascular injury by inducing the synthesis of proteoglycan core proteins that promote LDL accumulation at the subendothelial layers (11). Very little is known about fatty acid signal transduction. In different experimental systems, they have been postulated to bind to toll-like receptors, particularly TLR4 (39,40), peroxisome proliferator–activated receptor γ (41,42), or fatty acid–binding receptors (43) and to activate protein kinase C θ (44,45). These pathways converge on NF-κB activation and have been linked to inflammation and insulin resistance (30,46).

In conclusion, diabetic atheroma plaques have higher NEFA content than those from nondiabetic subjects. In vivo and in vitro experiments suggest that NEFA could be a key factor in the genesis of inflammation at the plaque.

ACKNOWLEDGMENTS

REFERENCES

1. World Health Organization: Diabetes: WHO Fact Sheet No. 312 [article online], 2009. Geneva, World Health Org. Available from www.who.int/mediacentre/factsheets/fs312/en/index.html
2. Basta G. Receptor for advanced glycation endproducts and atherosclerosis: from basic mechanisms to clinical implications. Atherosclerosis 2008;196:9–21
3. Price CL, Knight SC. Advanced glycation: a novel outlook on atherosclerosis. Curr Pharm Des 2007;13:3681–3687
4. Holland WL, Knotts TA, Chavez JA, Wang LP, Hoehn KL, Summers SA. Lipid mediators of insulin resistance. Nutr Rev 2007;65:S39–S46
5. Ruddock MW, Stein A, Landaker E, Park J, Cooksey RC, McClain D, Patti ME. Saturated fatty acids inhibit hepatic insulin action by modulating insulin receptor expression and post-receptor signalling. J Biochem 2008;144:599–607
6. Montecucco F, Steffens S, Mach F. Insulin resistance: a proinflammatory state mediated by lipid-induced signaling dysfunction and involved in atherosclerotic plaque instability. Mediators Inflamm 2008:767623, 2008
7. Rask-Madsen C, King GL. Proatherosclerotic mechanisms involving protein kinase C in diabetes and insulin resistance. Arterioscler Thromb Vasc Biol 2005;25:487–496
8. Chiarelli F, Marcovecchio ML. Insulin resistance and obesity in childhood. Eur J Endocrinol 2008;159(Suppl. 1):S67–S74
9. Wilding JP. The importance of free fatty acids in the development of type 2 diabetes. Diabet Med 2007;24:934–945
10. Armstrong KA, Hiremagalur B, Haluska BA, Campbell SB, Hawley CM, Marks L, Prins J, Johnson DW, Isbel NM. Free fatty acids are associated with obesity, insulin resistance, and atherosclerosis in renal transplant recipients. Transplantation 2005;80:937–944
11. Rodriguez-Lee M, Bondjers G, Camejo G. Fatty acid-induced atherogenic changes in extracellular matrix proteoglycans. Curr Opin Lipidol 2007;18:546–553
12. Brunelle A, Laprevote O. Recent advances in biological tissue imaging with time-of-flight secondary ion mass spectrometry: polyatomic ion sources, sample preparation, and applications. Curr Pharm Des 2007;13:3335–3343
13. Mas S, Touboul D, Brunelle A, Aragoncillo P, Egido J, Laprevote O, Vivanco F. Lipid cartography of atherosclerotic plaque by cluster-TOF-SIMS imaging. Analyst 2007;132:24–26
14. Touboul D, Brunelle A, Laprevote O. Structural analysis of secondary ions by post-source decay in time-of-flight secondary ion mass spectrometry. Rapid Commun Mass Spectrom 2006;20:703–709
15. Munoz-Garcia B, Martin-Ventura JL, Martinez E, Sanchez S, Hernandez G, Ortega L, Ortiz A, Egido J, Blanco-Colio LM. Fn14 is upregulated in cytokine-stimulated vascular smooth muscle cells and is expressed in human carotid atherosclerotic plaques: modulation by atorvastatin. Stroke 2006;37:2044–2053
16. Livak KJ, Schmittgen TD. Analysis of relative gene expression data using real-time quantitative PCR and the 2(-Delta Delta C(T)) Method. Methods 2001;25:402–408
17. Hernandez-Presa MA, Martin-Ventura JL, Ortego M, Gomez-Hernandez A, Tunon J, Hernandez-Vargas P, Blanco-Colio LM, Mas S, Aparicio C, Ortega L, Vivanco F, Gerique JG, Diaz C, Hernandez G, Egido J. Atorvastatin reduces the expression of cyclooxygenase-2 in a rabbit model of atherosclerosis and in cultured vascular smooth muscle cells. Atherosclerosis 2002;160:49–58
18. Hernandez-Presa MA, Ortego M, Tunon J, Martin-Ventura JL, Mas S, Blanco-Colio LM, Aparicio C, Ortega L, Gomez-Gerique J, Vivanco F, Egido J. Simvastatin reduces NF-kappaB activity in peripheral mononuclear and in plaque cells of rabbit atheroma more markedly than lipid lowering diet. Cardiovasc Res 2003;57:168–177
19. Hernandez-Presa MA, Gomez-Guerrero C, Egido J. In situ non-radioactive detection of nuclear factors in paraffin sections by Southwestern histochemistry. Kidney Int 1999;55:209–214
20. Martin-Ventura JL, Blanco-Colio LM, Gomez-Hernandez A, Munoz-Garcia B, Vega M, Serrano J, Ortega L, Hernandez G, Tunon J, Egido J. Intensive treatment with atorvastatin reduces inflammation in mononuclear cells and human atherosclerotic lesions in one month. Stroke 2005;36:1796–1800
21. Erkelens DW. Diabetic dyslipidaemia. Eur Heart J 1998;19(Suppl. H):H27–H40
22. Schwertner HA, Mosser EL. Comparison of lipid fatty acids on a concentration basis vs weight percentage basis in patients with and without coronary artery disease or diabetes. Clin Chem 1993;39:659–663
23. Goldberg IJ, Merkel M. Lipoprotein lipase: physiology, biochemistry, and molecular biology. Front Biosci 2001;6:D388–D405
24. Bartels ED, Nielsen JE, Lindegaard ML, Hulten LM, Schroeder TV, Nielsen LB. Endothelial lipase is highly expressed in macrophages in advanced human atherosclerotic lesions. Atherosclerosis 2007;195:e42–e49
25. Moreno PR, Murcia AM, Palacios IF, Leon MN, Bernardi VH, Fuster V, Fallon JT. Coronary composition and macrophage infiltration in atherectomy specimens from patients with diabetes mellitus. Circulation 2000;102:2180–2184
26. Ping D, Boekhoudt GH, Rogers EM, Boss JM. Nuclear factor-kappa B p65 mediates the assembly and activation of the TNF-responsive element of the murine monocyte chemoattractant-1 gene. J Immunol 1999;162:727–734
27. Qiu G, Hill JS. Atorvastatin decreases lipoprotein lipase and endothelial lipase expression in human THP-1 macrophages. J Lipid Res 2007;48:2112–2122
28. Bork PM, Schmitz ML, Kuhnt M, Escher C, Heinrich M. Sesquiterpene lactone containing Mexican Indian medicinal plants and pure sesquiterpene lactones as potent inhibitors of transcription factor NF-kappaB. FEBS Lett 1997;402:85–90
29. Lopez-Franco O, Hernandez-Vargas P, Ortiz-Munoz G, Sanjuan G, Suzuki Y, Ortega L, Blanco J, Egido J, Gomez-Guerrero C. Parthenolide modulates the NF-kappaB-mediated inflammatory responses in experimental atherosclerosis. Arterioscler Thromb Vasc Biol 2006;26:1864–1870
30. Clee SM, Bissada N, Miao F, Miao L, Marais AD, Henderson HE, Steures P, McManus J, McManus B, LeBoeuf RC, Kastelein JJ, Hayden MR. Plasma and vessel wall lipoprotein lipase have different roles in atherosclerosis. J Lipid Res 2000;41:521–531
31. Rader DJ, Jaye M. Endothelial lipase: a new member of the triglyceride lipase gene family. Curr Opin Lipidol 2000;11:141–147
32. Virani SS, Nambi V. The role of lipoprotein-associated phospholipase A2 as a marker for atherosclerosis. Curr Atheroscler Rep 2007;9:97–103
33. Carlquist JF, Muhlestein JB, Anderson JL. Lipoprotein-associated phospholipase A2: a new biomarker for cardiovascular risk assessment and potential therapeutic target. Expert Rev Mol Diagn 2007;7:511–517
34. Oram JF, Bornfeldt KE. Direct effects of long-chain non-esterified fatty acids on vascular cells and their relevance to macrovascular complications of diabetes. Front Biosci 2004;9:1240–1253
35. Ichikawa T, Liang J, Kitajima S, Koike T, Wang X, Sun H, Morimoto M,

Shikama H, Watanabe T, Yamada N, Fan J. Macrophage-derived lipoprotein lipase increases aortic atherosclerosis in cholesterol-fed Tg rabbits. Atherosclerosis 2005;179:87–95

36. Haversen L, Danielsson KN, Fogelstrand L, Wiklund O. Induction of proinflammatory cytokines by long-chain saturated fatty acids in human macrophages. Atherosclerosis 2009;202:382–393

37. Itani SI, Ruderman NB, Schmieder F, Boden G. Lipid-induced insulin resistance in human muscle is associated with changes in diacylglycerol, protein kinase C, and IκB-α. Diabetes 2002;51:2005–2011

38. Boden G, She P, Mozzoli M, Cheung P, Gumireddy K, Reddy P, Xiang X, Luo Z, Ruderman N. Free fatty acids produce insulin resistance and activate the proinflammatory nuclear factor-κB pathway in rat liver. Diabetes 2005;54:3458–3465

39. Suganami T, Tanimoto-Koyama K, Nishida J, Itoh M, Yuan X, Mizuarai S, Kotani H, Yamaoka S, Miyake K, Aoe S, Kamei Y, Ogawa Y. Role of the toll-like receptor 4/NF-kappaB pathway in saturated fatty acid-induced inflammatory changes in the interaction between adipocytes and macrophages. Arterioscler Thromb Vasc Biol 2007;27:84–91

40. Kim F, Pham M, Luttrell I, Bannerman DD, Tupper J, Thaler J, Hawn TR, Raines EW, Schwartz MW. Toll-like receptor-4 mediates vascular inflammation and insulin resistance in diet-induced obesity. Circ Res 2007;100:1589–1596

41. Hancock CR, Han DH, Chen M, Terada S, Yasuda T, Wright DC, Holloszy JO. High-fat diets cause insulin resistance despite an increase in muscle mitochondria. Proc Natl Acad Sci U S A 2008;105:7815–7820

42. Vandewalle B, Moerman E, Lefebvre B, Defrance F, Gmyr V, Lukowiak B, Kerr Conte J, Pattou F. PPARgamma-dependent and -independent effects of rosiglitazone on lipotoxic human pancreatic islets. Biochem Biophys Res Commun 2008;366:1096–1101

43. Swaminath G. Fatty acid binding receptors and their physiological role in type 2 diabetes. Arch Pharm (Weinheim) 2008;341:753–761

44. Ragheb R, Medhat AM, Shanab GM, Seoudi DM, Fantus IG. Links between enhanced fatty acid flux, protein kinase C and NFkappaB activation, and apoB-lipoprotein production in the fructose-fed hamster model of insulin resistance. Biochem Biophys Res Commun 2008;370:134–139

45. Dey D, Basu D, Roy SS, Bandyopadhyay A, Bhattacharya S. Involvement of novel PKC isoforms in FFA induced defects in insulin signaling. Mol Cell Endocrinol 2006;246:60–64

46. Wunderlich FT, Luedde T, Singer S, Schmidt-Supprian M, Baumgartl J, Schirmacher P, Pasparakis M, Bruning JC. Hepatic NF-kappa B essential modulator deficiency prevents obesity-induced insulin resistance but synergizes with high-fat feeding in tumorigenesis. Proc Natl Acad Sci U S A 2008;105:1297–1302